Research Article

Qiuyang Zhang#, Li Zhang#, Minhui Yang, Qingxiang Hong, Zhongmei Yang, Sen Liu, Qingping Xiong, and Changjiang Pan*

Construction of Chi(Zn/BMP2)/HA composite coating on AZ31B magnesium alloy surface to improve the corrosion resistance and biocompatibility

https://doi.org/10.1515/ntrev-2021-0063
received June 18, 2021; accepted August 11, 2021

Abstract: As biodegradable orthopedic implant materials, magnesium alloys have been attracted enough attentions recently. However, too fast degradation *in vivo*, limited biocompatibilities, and insufficient antibacterial properties are three main challenges at present. In order to solve these problems, a multifunctional composite coating of Chi(Zn/BMP2)/HA was constructed on AZ31B magnesium alloy surface, successively by the alkali heating treatment, self-assembly of 16-phosphonyl-hexadecanoic acid, *in situ* immobilization of Chi(Zn/BMP2) (chitosan, zinc ions, and bone morphogenetic protein 2), and the deposition of HA (hydroxyapatite). The results of ATR-FTIR (attenuated total reflection Fourier transform infrared spectrum) spectra and elemental compositions confirmed that 16-phosphonyl-hexadecanoic acid, Chi(Zn/BMP2), and HA were successfully immobilized on the surface. Compared with Mg, Mg-OH, Mg-16, and Mg-Chi(Zn/BMP2), Mg-Chi(Zn/BMP2)/HA with the concave–convex structure surface significantly enhanced the hydrophilicity and corrosion resistance. On the other hand, Mg-Chi(Zn/BMP2)/HA coating also showed excellent biocompatibilities, which not only significantly promoted the osteoblast adhesion and proliferation, but also upregulated ALP and OCN expression of osteoblasts. Furthermore, due to the synergistic antibacterial effect of zinc ions and chitosan, Mg-Chi(Zn/BMP2)/HA showed a good antibacterial property against *Escherichia coli* (*E. coli*). Therefore, it can be said that the method used in this work has a good application prospect in improving the corrosion resistance, biocompatibility of magnesium alloys, and inhibiting infections against *E. coli*.

Keywords: magnesium alloy, multifunctional composite coatings, corrosion resistance, biocompatibilities, antibacterial properties

1 Introduction

There are increasing demands on clinical implants for orthopedic diseases [1]. Compared with ceramics and polymers, biomedical metals are more suitable for hard-tissue implants, especially in load-bearing application, owing to their excellent strength and toughness [2,3]. Stainless steels, cobalt–chromium-based alloys, and titanium alloys are commonly used to repair serious bone fracture or replace the bone tissue. However, specific drawbacks limit their widespread use. First, their mismatched elastic modus with natural bone tissue contributes to occurrence of the stress-shielding effect and restrains the growth of new bone [4]. Second, harmful metallic ions or particles released through corrosion or wear can lead to inflammation, cell apoptosis, and other destructive tissue reactions [5,6]. Third, the three metallic materials, called as permanent rigid metals, must be removed from the human body by a second surgical

# These authors contributed equally to this work.

* **Corresponding author: Changjiang Pan,** Faculty of Mechanical and Material Engineering, Jiangsu Provincial Engineering Research Center for Biomedical Materials and Advanced Medical Devices, Huaiyin Institute of Technology, Huai'an 223003, China, e-mail: panchangjiang@hyit.edu.cn
Qiuyang Zhang, Minhui Yang, Qingxiang Hong, Zhongmei Yang, Sen Liu: Faculty of Mechanical and Material Engineering, Jiangsu Provincial Engineering Research Center for Biomedical Materials and Advanced Medical Devices, Huaiyin Institute of Technology, Huai'an 223003, China
Li Zhang: The Affiliated Huai'an Hospital of Xuzhou Medical University, Huai'an 223003, China
Qingping Xiong: Faculty of Chemical Engineering, Huaiyin Institute of Technology, Huai'an 223003, China

procedure after tissues have healed [7]. The repeated surgery increases morbidity and health costs of patients. Therefore, the promising bone substitutes should possess good biocompatibility, biodegradability, and matching mechanical properties with natural bones.

Recently, magnesium alloys have become more attractive in the field of bone repair and regeneration [1–3,7–10]. Magnesium and its alloys possess unique mechanical properties. The specific density of magnesium and its alloys (1.7 g/cm^3) is very similar to that of human calvarium bone (1.75 g/cm^3), the elastic modulus of pure magnesium (45 GPa) closely matches that of human bone (40–57 GPa) [2], and the compressive and tensile strengths are higher relative to natural bones [1]. These unique mechanical properties of magnesium alloys can overcome the shortcomings of traditional orthopedic metals by restricting stress-shielding effect during load transfer at the interface of implant to bone. Moreover, magnesium is the fourth most abundant element in the human body and is largely stored in bone tissues [2]. Simultaneously, magnesium participates in the metabolic process and plays an important role in the regulation of ion channels, DNA stabilization, enzyme activation, and stimulation of cell growth and proliferation [8]. Mg ions in human body can induce osteoblast differentiation and accelerate healing in bone diseases [9,10]. Many evidences also demonstrate that magnesium and its alloys as promising orthopedic implants are very biocompatible [2,3]. Additionally, magnesium is a biodegradable and absorbable metal with a lower standard electrode potential than hydrogen [1]; therefore, they can be readily dissolved or corroded in aqueous solutions especially that containing chloride ions. If magnesium-based materials were implanted into a body, they can be completely degraded under physiological environment. The degradation products can be absorbed by the human body or excreted *via* metabolism [11,12] and thus avoid the second surgical procedure. Compared with permanent implants, biodegradable magnesium alloys are thus preferred to be desirable implants with a temporary function.

However, the clinical applications of the biodegradable magnesium alloys face some challenges. One of major drawbacks is its low corrosion resistance especially in electrolytic and aqueous environments. As reported, magnesium alloys can be easily corroded under physiological environment, but the corrosion rate is so quick that they lose the mechanical integrity before the tissue has sufficiently healed [1]. The seriously corroded magnesium alloys could not provide enough structural support for the injured tissue during service, finally leading to the implant failure. Meanwhile, the corrosion products of $Mg(OH)_2$ and hydrogen gas also have side effects to some degree *in vivo*. For example, hydrogen gas evolves too fast to be immediately dealt with by the host tissue [13], resulting in excessively accumulating and subcutaneously dispersing of visible gas bubbles. High concentration of hydrogen gas might cause health risks in patients according to reported studies performed in rats [14]. The rapid formation of $Mg(OH)_2$ increases the pH in the vicinity of the implant and causes the local high alkalization [15], further affecting the process of physiological activity. Massive $Mg(OH)_2$ can also bring severe toxicities to prevent the tissue healing. Besides, the insufficient surface bioactivities of magnesium alloys need to be further improved [16], so that magnesium implants are expected to be more compatible with surrounding tissues [17–22]. In terms of orthopedic implants, desirable magnesium alloys are also expected to promote bone healing and osteoblast differentiation. In addition, the antibacterial capability of magnesium-based biomaterials should also be considered. Magnesium alloys are usually considered to have excellent antibacterial properties *in vitro* [23,24]. However, the recent studies [25,26] found that magnesium alloys have antimicrobial properties *in vitro* but not *in vivo*. To improve the antibacterial capability of magnesium alloys is also imperative. Therefore, controllable corrosion rates, excellent osteogenic activity, and improved antibacterial properties are the prerequisites for magnesium alloys being safely used as orthopedics implants.

The properties mentioned above are closely related to magnesium alloy surfaces. In recently years, many studies [17–22] have focused on improving the surface properties. Gao *et al.* [17] deposited bioactive multilayer coating of chitosan-functionalized graphene oxide and heparin on AZ31B alloy through layer by layer to improve the corrosion resistance and biocompatibility. Gao *et al.* [18] immersed AZ60 Mg alloy into the chemical solution to obtain a CaP coating, which not only significantly improved the cell adhesion, proliferation, and differentiation of osteoblasts, but also provided a better biodegradation behavior. Wei *et al.* [19] introduced NH^{2+} onto the AZ31 Mg alloy surface by ions implantation to enhance the corrosion resistance and biocompatibility. In the study of Wu *et al.* [20], a hybrid coating, consisting of seal porous layered double hydroxide coating and poly-L-glutamic acid coating synthesized by hydrothermal treatment and vacuum freeze-drying method, was immobilized on AZ31 magnesium alloy. The hybrid coating effectively provided the corrosion protection and acceptable cytocompatibility for mouse embryonic fibroblasts. Xue *et al.* [21] designed a cross-linked ciprofloxacin and polymethyltrimethoxysilane with an inner micro-arc oxidation coating on AZ31 alloy, to enhance corrosion resistance and antibacterial ability. Wang *et al.* [22] developed a

composite coating on AZ31 alloy surface with a combination of micro-arc oxidation and self-assembly of polyethyleneimine and Ag nanoparticles, which effectively improved the corrosion resistance and antibacterial properties.

Although coating technology (deposition, ions implantation, hydrothermal treatment, vacuum freeze-drying method, and so on) had been used to solve some problems in above researches [17–22], the corrosion resistance, biocompatibility, and antibacterial properties of magnesium alloys seemed not to be improved at the same time by one coating. As known, these properties were indispensable for orthopedic implant materials. Therefore, to synergistically enhance the corrosion resistance, biocompatibility, and antibacterial properties, it is essential to construct a multifunctional coating. Bone morphogenetic protein 2 (BMP2) is a special bone growth factor and plays a significant role in enhancing osteogenesis/osseointegration and ultimately inducing the formation of bone [27]. Zinc ions also take effect in the osteoblast growth, such as inhibiting the osteoclast activities and promoting the osteoblast differentiation. Zinc ions can inhibit the formation of bacterial plaque and have a stronger antibacterial effect [28]. Chitosan (Chi) is a biodegradable polysaccharide with good biocompatibilities and antibacterial properties [29]. It can not only promote cell adhesion and proliferation, but also has a good ability to chelate metallic ions [30]. Moreover, chitosan, containing lots of positive charges in electrolyte solution, is also widely used in constructing bioactive polyelectrolyte multilayer. Additionally, hydroxyapatite (HA) can induce the growth of surrounding tissues and form a strong chemical bond directly with host bones [31]. It has been widely applied in dentistry, antitumor drug carriers, and orthopedic repair.

In this work, a multifunctional bioactive coating of Chi(Zn/BMP2)/HA on AZ31B magnesium alloy was constructed to synergistically improve the corrosion resistance, biocompatibilities, and antibacterial properties. Chitosan was first used to bind BMP2 and chelate zinc ions to prepare a complex of Chi(Zn/BMP2). Then, the alkali heating treatment was used to activate the magnesium alloy surface, and 16-phosphonyl-hexadecanoic acid was immobilized by self-assembly to further enhance the corrosion resistance and introduce bioactive molecules. Subsequently, Chi(Zn/BMP2) was covalently grafted on the surface of activated AZ31B magnesium alloy. Finally, HA was deposited. The surface characteristics, corrosion resistance, *in vitro* cytocompatibility, and antibacterial properties of the complex coating on AZ31B magnesium alloy were investigated in detail.

2 Materials and methods

2.1 Constructing Chi(Zn/BMP2)/HA coating on AZ31B magnesium alloy surfaces

First, the Chi(Zn/BMP2) complex solution was prepared by thoroughly mixing 5 mg/mL chitosan (Adamas Reagent Co., Ltd, in pH = 5 acetic acid), 5 mM zinc acetate, and 50 ng/mL BMP2 (Invitrogen Co., Ltd., Shanghai) with the volume ratio of 10:1:1. The AZ31B magnesium alloy plates (Dongguan You'an Metal Co., Ltd., China) with 10 mm diameter and 3 mm thickness were polished to mirror and then cleaned by acetone, ethanol, and deionized water. The plates were immersed in 3 M NaOH solution for 24 h at 75°C, and the obtained samples were marked as Mg-OH. Afterwards, these samples were further dipped into 5 mM 16-phosphonyl-hexadecanoic acid (Sigma-Aldrich, China) for 24 h under shaking condition. The samples were taken out and then treated for 12 h at 120°C in order to enhance the binding force of 16-phosphonyl-hexadecanoic acid. After being cleaned and dried, the samples were marked as Mg-16. The Mg-16 was incubated with 10 mM EDC/NHS (1-(3-dimethylaminopropyl)-3-ethylcarbodiimide hydrochloride/*N*-hydroxysuccinimide) (Sigma-Aldrich, China) solution to activate carboxyl groups of magnesium alloy surfaces, followed by being immersed in the as-prepared Chi(Zn/BMP2) complex solution for 1 h. The samples were washed, dried, and then denoted as Mg-Chi(Zn/BMP2). Finally, the Mg-Chi(Zn/BMP2) was incubated in 2 mg/mL HA nanoparticle (average diameter 40 nm) solution to form the HA layer on the surfaces, and the final samples were labelled as Mg-Chi(Zn/BMP2)/HA.

2.2 Surface characterization

The surface chemical groups of magnesium alloy were characterized by attenuated total reflection Fourier transform infrared spectroscopy (ATR-FTIR, TENSOR 27, Bruker of Germany) at room temperature with a scanning range of 4,000–650 cm^{-1}. The surface morphologies of the samples were observed by scanning electron microscopy (SEM, FEI Quata 250, USA). Energy dispersive spectroscopy (EDS, IMA X-MAX 20, Britain) was used to determine the surface element compositions. The water contact angle (DSA25, Krüss GmbH, Germany) was measured to characterize the surface hydrophilicity of the different samples; three samples were measured and the values were averaged.

2.3 Release profiles of BMP2 and Zn^{2+}

Mg, Mg-Chi(Zn/BMP2), and Mg-Chi(Zn/BMP2)/HA were sealed with silicone rubber and then respectively incubated with 20 mL SBF solution for different times. At each predetermined time, 100 μL solution was drawn for measurements, and the medium was supplemented with 100 μL fresh SBF.

The released BMP2 was measured by enzyme-linked immunosorbent assay (ELISA). Briefly, 100 μL standard solution and 100 μL sample solution were respectively added into the test plates. After being cultivated 90 min at 37°C, 100 μL of Biotinylated anti-mouse BMP2 antibody was added to incubate 60 min, followed by adding 100 μL Avidin-Biotin-Peroxidase Complex solution. Finally, 90 μL chromogenic agent was added and incubated for 20 min, and the terminating solution was added to stop the reaction. The absorbance at 450 nm was measured and the concentration of BMP2 was calculated according to the standard curve.

The release concentration of Zn^{2+} in the medium was detected by an Optima 7000 DV Inductively Coupled Plasma Luminescence Spectroscopy (PerkinElmer), and the ions concentrations were calculated according to the standard curves. The release profile curves were plotted according to the ion concentrations.

2.4 Electrochemical corrosion behaviors

The potentiodynamic scanning polarization curve and alternative circuit impedance spectroscopy were performed on an electrochemical workstation (CHI Instruments, Inc., Shanghai, China) to characterize the electrochemical corrosion behaviors of the control and modified magnesium alloys. The standard three-electrode system was used, the sample as the working electrode, the platinum wire as the auxiliary electrode, and the Ag/AgCl as the reference electrode. The test solution was Hank's simulated body fluid (SBF, composition: NaCl 8 g/L, KCl 0.4 g/L, $NaHCO_3$ 0.35 g/L, $CaCl_2$ 0.14 g/L, Na_2HPO_4 0.06 g/L, KH_2PO_4 0.06 g/L, $MgSO_4 \cdot 7H_2O$ 0.01 g/L, glucose 1 g/L). The sample was sealed with silicone rubber using copper wire as conductor, and the exposed area was 1 cm^2. For the polarization curve, the sample was immersed in SBF before testing until the open circuit potential was stable, and the scanning speed was 1 mV/s. The corrosion current was fitted by Tafel extrapolation method and the corrosion current density was calculated. For EIS measurement, the scanning scope was 10^5–0.1 Hz with a disturbance signal of sinusoidal AC potential with an amplitude of 10 mV.

2.5 The degradable behaviors of the modified magnesium alloys

The degradable behaviors of the control and modified magnesium alloys were investigated by pH changes and Mg^{2+} release from the medium. In order to measure the pH value changes, the samples were sealed with silicone rubber and then respectively incubated with 20 mL SBF solution for different times; the medium was refreshed every 2 days. The pH values were measured at 3, 6, 12 h, 1, 2, 4, 7, 10, and 14 days, respectively. Three parallel samples were used and the average values were calculated. For Mg^{2+} release, the sample was sealed by silicon rubber and then incubated with SBF solution for 3 h, 1, 3, 5, and 7 days, respectively. At each time, 100 μL medium was taken out and supplemented by 100 μL fresh SBF. The Mg^{2+} concentration was detected by an Optima 7000 DV Inductively Coupled Plasma Luminescence Spectroscopy (PerkinElmer). The ions concentrations were used to plot the release profile curves.

2.6 Growth behaviors of osteoblasts

2.6.1 Cell attachment and proliferation

To investigate the behaviors of osteoblasts on different magnesium alloy surfaces, the samples were sealed by silicone rubber and incubated with 0.5 mL osteoblasts suspension (5×10^4 cells/mL, ECV304, Cobioer, Nanjing, China) and 1.5 mL medium (DMEM F12 containing 5% FBS and 1% penicillin–streptomycin) at 37°C with 5% CO_2. After 1 or 3 days, the samples were washed twice by normal saline. The attached cells were fixed in 2.5% glutaraldehyde for 3 h at 4°C and then stained successively with 200 μL rhodamine (Aladdin Biochemical Technology Co., Ltd., 1:1,000 in PBS) and 200 μL 4′,6-diamidino-2-phenylindole (DAPI, Aladdin Biochemical Technology Co., Ltd., 1:400 in PBS). The stained samples were washed twice by normal saline again and inspected under a Zeiss Inverted A2 fluorescence microscope.

The proliferation of osteoblasts was estimated by CCK-8 (Cell Counting Kit-8). Briefly, the sample was incubated with osteoblasts in the same way for 1 and 3 days, respectively, and then the medium was removed and replaced by fresh 10% CCK-8 solution. After incubation at 37°C for 3.5 h, the absorbance of the medium was measured at 450 nm with a microplate reader (Bio-Tek, Eons).

2.6.2 ALP and OCN secretion of osteoblasts

The alkaline phosphatase (ALP) and osteocalcin (OCN) activities of osteoblasts were determined by ELISA. 0.5 mL

osteoblasts cells suspensions (5×10^4 cells/mL) and 1.5 mL culture medium were seeded on different magnesium alloys and cultured for 1–3 days at 37°C. The supernatant was diluted 5 times and then incubated 30 min at 37°C. The chromogenic agents and terminating solution were successively added. The optical density value was measured at 450 nm by the microplate reader. The ALP and OCN concentrations were determined according to the standard curves.

2.7 Antibacterial activities

2.7.1 Bacteria adhesion

Escherichia coli (*E. coli*, ATCC25922) was cultured and diluted with nutrient broth to obtain a test inoculum with a concentration of 5×10^5 cells/mL. A 100 µL bacteria solution was distributed evenly onto each surface to incubate 2 h at 37°C. After being washed thrice by PBS, the attached bacteria were fixed by 2.5% glutaraldehyde followed by dehydrating with 50, 70, 90, and 100% ethanol solutions for 10 min each time. The adhesion of bacteria was observed by scanning electron microscope after spraying gold layer on the surfaces.

2.7.2 Antibacterial test

The evaluation on bactericidal activities was carried out according to ISO22196-2007 and *E. coli* (ATCC 25922) was chosen for the antimicrobial tests. *E. coli* was precultured and diluted with nutrient broth to obtain a test inoculum with a concentration of 5×10^5 cells/mL. The magnesium alloys before and after being modified were sterilized by UV and placed in the sterilized Petri dishes. A 0.2 mL test inoculum was dropped onto the surfaces of magnesium alloys and incubated for 24 h at 37°C. Finally, the surviving bacteria on the surfaces of samples were collected into a new Petri dish and diluted 10 times. A 100 µL diluted solution was dropped on the agar, which was then incubated at 37°C for 24 h. The bacterial colonies were observed and photographed.

2.8 Statistical analysis

For each experiment, three parallel samples were measured; the data were averaged and expressed as mean ± standard derivation (SD). The results of water contact angle and cell assay were statistically analyzed by SPSS software using one-way ANOVA, and $p < 0.05$ is considered to be statistically significant.

3 Results and discussion

3.1 Surface characteristics

Figure 1a shows the representative surface topographies of the different samples. Table 1 presents the elemental compositions on the surfaces. It can be seen that the polished magnesium alloy possessed a smooth surface (Figure 1a(a)). A large amount of Mg as well as a little of Al, Zn, and O can be detected by EDS. Al and Zn are the inherent components of AZ31B alloy, while the existence of O implied the slight oxidation of magnesium alloy surface. After 24 h alkali heat treatment, the surface morphology of Mg-OH did not change significantly (Figure 1a(b)), but the contents of O substantially increased up to 33.51 at%. For the sample of Mg-16, some white aggregates started to occur. A large amount of C element (22.5 at%) was found first, which should be derived from 16-phosphonyl-hexadecanoic acid. After the immobilization of Chi(Zn/BMP2) complex, massive zinc-containing particles were observed (Figure 1a(d)), which can be attributed to the chelation of chitosan to Zn^{2+}. After the deposition of hydroxyapatite, a compact coating with the concave–convex structure covered the surface (Figure 1a(e)). This was also confirmed by the EDS analysis on Ca and P elements.

Figure 1b illustrates the ATR-FTIR spectra of surface chemical groups. As expected, there was almost no infrared absorption for the pristine magnesium alloy. For Mg-OH, the stretching vibration of –OH can be detected at 3,700 cm^{-1}, indicating that many hydroxyl groups were successfully introduced onto the surface after alkali heat treatment. For Mg-16, the strong absorption peaks at 1,710, 2,850, and 2,920 cm^{-1}, corresponding to C═O, $-CH_3$, and s-CH_2– groups, respectively, suggested that 16-phosphonyl-hexadecanoic acid was successfully immobilized on the surface. For Mg-Chi(Zn/BMP2), besides the peaks of –OH at 3,700 cm^{-1} and C═O at 1,710 cm^{-1}, the absorption peak of C═O also appeared at 1,653 cm^{-1}. This was attributed to the amide reaction between $-NH_2$ group from chitosan and –COOH group from 16-phosphonyl-hexadecanoic acid. After the deposition of hydroxyapatite, the absorption peak at 3,700 cm^{-1} further strengthened because of increasing –OH groups. Additionally, another intense peak of P–O in phosphate radical can be also detected at 1,040 cm^{-1}.

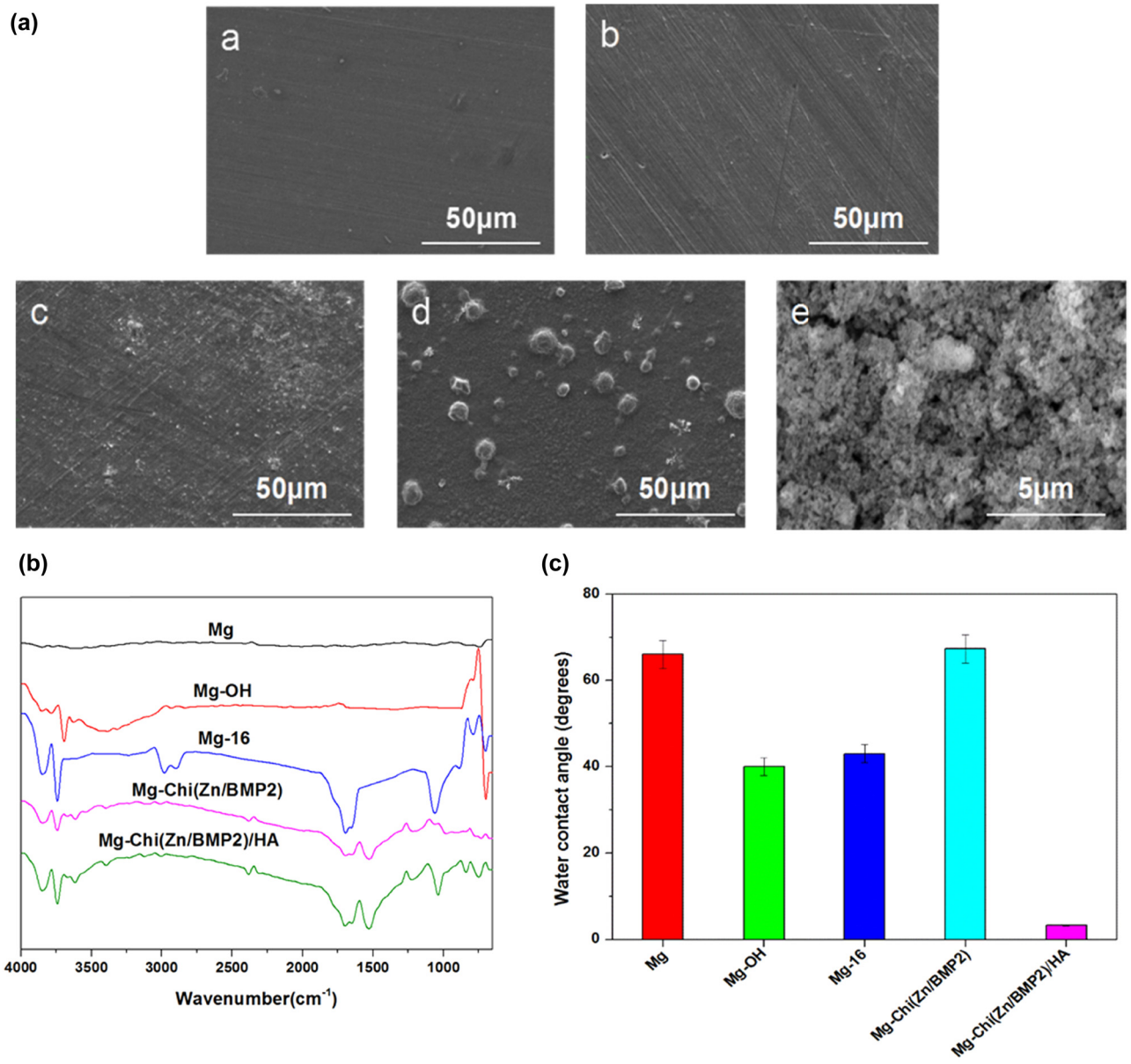

Figure 1: The representative SEM images ((a), Mg (a), Mg-OH (b), Mg-16 (c), Mg-Chi(Zn/BMP2) (d), Mg-Chi(Zn/BMP2)/HA (e)), ATR-FTIR spectra (b), and water contact angles (c) of the different samples.

Table 1: Elemental compositions of the different samples

Samples	Atomic concentration (at%)							
	Mg	O	Al	C	N	Zn	Ca	P
Mg	92.67	3.77	2.73	—	—	0.83	—	—
Mg-OH	64.55	33.51	1.36	—	—	0.58	—	—
Mg-16	51.56	25.94	—	22.50	—	—	—	—
Mg-Chi(Zn/BMP2)	35.28	33.69	—	18.69	5.04	7.30	—	—
Mg-Chi(Zn/BMP2)/HA	1.46	38.24	—	7.74	1.35	0.65	31.38	19.18

Figure 1c reveals the results of the water contact angles of different samples. The pristine magnesium alloy exhibited relatively poor hydrophilicity with a water contact angle of around 66°, which is similar to the existing results [19,32]. The alkali heat treatment can produce many –OH groups on the surface, which can interact with water molecules through a hydrogen bond to enhance the hydrophilicity [33]; therefore, the water contact angle decreased to 40°. After self-assembly, the phosphonyl groups from 16-phosphonyl-hexadecanoic acid interacted with –OH groups by the dehydration reaction, leading to the consumption of –OH and the introduction of $-PO_3$ and –COOH. Thus, the water contact angle of Mg-16 was slightly elevated. For Mg-Chi(Zn/BMP2), in spite of many hydrophilic groups of –OH in chitosan, the water contact angle still increased significantly after the complex coating formed on the surface. This can contribute to high value of water contact angle of pure chitosan, which is close to 70°[34]. After depositing hydroxyapatite, the reintroduction of many hydrophilic –OH groups and the concave–convex structure of hydroxyapatite enlarging the contact area between the material and water lead to excellent hydrophilicity. Therefore, the water contact angle of Mg-Chi(Zn/BMP2)/HA sharply decreased to 3.3°.

3.2 Release profiles of Zn^{2+} and BMP2

Figure 2 shows the release profiles of Zn^{2+} and BMP2 over 7 days. The release behavior of Zn^{2+} from the pristine magnesium alloy was also investigated as comparison. Owing to the low content of Zn in AZ31B alloy (as listed in Table 1), the released zinc ion concentration from Mg alloy was only about 3 ng/mL in 1 day, and slowly increased over 7 days. The similar release behaviors of Zn ions from as-received Mg alloys were also found in other studies [35,36]. For Mg-Chi(Zn/BMP2) and Mg-Chi (Zn/BMP2)/HA, the release amount of zinc ions was very close to each other and much higher than the pristine Mg. It is suggested that HA deposition had almost no side effects on the release behavior of zinc ions. In 1 day, the concentrations got up to 64 and 62 ng/mL, respectively. As the immersion time increased, the zinc ions were continuously released. By the seventh day, the content of zinc ions from Mg-Chi(Zn/BMP2)/HA achieved 116 ng/mL. It is expected that the sustained release of zinc ions can have a long-term antibacterial effect [28].

According to Figure 2b, the release behavior of BMP2 totally differed from that of Zn^{2+}. In 1 day, there was almost no clear differences between Mg-Chi(Zn/BMP2) and Mg-Chi(Zn/BMP2)/HA. The BMP2 release amount was about 10 ng/mL. However, with the immersion time increasing, the release rate of BMP2 was different between Mg-Chi(Zn/BMP2)/HA and Mg-Chi(Zn/BMP2). The release concentration of BMP2 was lower for Mg-Chi(Zn/BMP2)/HA, which can be contributed to the hindrance of HA compact coating. This implies that the Mg-Chi(Zn/BMP2)/HA complex coating would have a greater advantage towards osteoblast growth, proliferation, and adhesion. The HA compact coating on the surface easily obstructed the release of BMP2 to some extent, because BMP2 has a larger molecular weight than Zn, resulting in the slow release of BMP2 and the rapid release of Zn^{2+} from the coating.

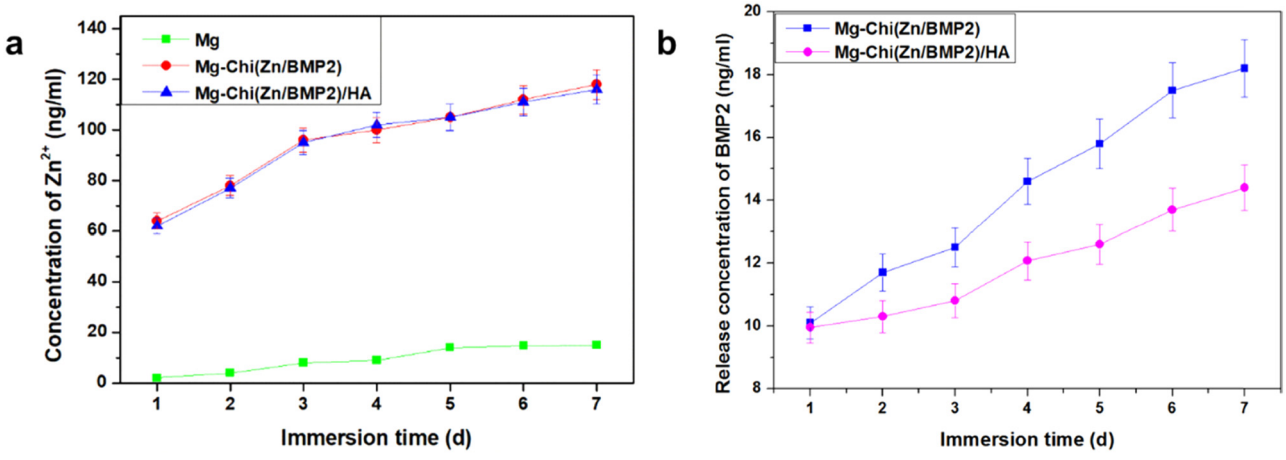

Figure 2: The release profiles of Zn^{2+} (a) and BMP2 (b) over 7 days.

3.3 Electrochemical corrosion and degradation behaviors

Figure 3a shows the electrochemical polarization curves. Table 2 lists the corresponding corrosion parameters. It is clear that the pristine magnesium alloy had the lowest corrosion potential (–1.648 V), the largest corrosion current density (2.340×10^{-5} A/cm^2), and annual corrosion depth (0.54 mm/year) among all samples, indicating a poor corrosion resistance and a severe corrosion tendency in physiological environment. After alkali heat treatment, the formed $Mg(OH)_2$ layer can isolate the substrate from the corrosion medium and prevent the corrosive medium penetrating the magnesium matrix. Thus, the corrosion potential was increased to some extent, and the corrosion current density and annual corrosion depth were decreased, as shown in Figure 3a and Table 2. For Mg-16, the corrosion potential was further increased to –1.490 V, and the corrosion current density and annual corrosion depth were also decreased after the self-assembly of 16-phosphonyl-hexadecanoic acid. The improved corrosion resistance can be attributed to two reasons. The first was a partial phosphating effect. The phosphonyl groups from 16-phosphonyl-hexadecanoic acid can be immobilized on the surface by the dehydration reaction with –OH of Mg-OH, thus a partial phosphating effect was also produced on the surface to enhance the corrosion resistance. The second was the covering effect of the molecules. Moreover, the carboxyl groups from 16-phosphonyl-hexadecanoic acid molecules on the surface made Mg-16 negatively charged, hindering the invasive corrosion of chloride and other anion ions. After covalently immobilizing Chi(Zn/BMP2) with Mg-16, the corrosion current density was increased to –1.418 V, and the corrosion current density and corrosion depth were decreased to 3.528×10^{-5} A/cm^2 and 0.08 mm/year, respectively. This was ascribed to the complex coating separating the substrate from Hank's simulated body fluid, avoiding the direct pitting of magnesium alloy by chloride ions. At the same time, the amino groups of chitosan are positively charged, promoting the combination with anion ions and hindering their invasive corrosion. In addition, the chitosan cannot be readily degraded under alkaline conditions (caused by magnesium alloy dissolution), and thus the stability of coating was also improved *in vivo* environments [30]. After being deposited onto Chi(Zn/BMP2), the hydroxyapatite covered the surfaces and formed a compact coating, which remarkably improved the corrosion resistance and slowed down the corrosion rate of magnesium alloy. As shown in Figure 3a and Table 2, the corrosion potential was increased to –1.408 V, and the corrosion current density was decreased by an order as compared to the control Mg and annual corrosion depth was merely 0.06 mm/year.

Table 2: Corrosion potential, corrosion current density, and annual corrosion depth of the different samples

Samples	E_{corr} (V)	I_{corr} (A cm^{-2})	d (mm/year)
Mg	–1.648	2.340×10^{-5}	0.54
Mg-OH	–1.615	9.827×10^{-6}	0.22
Mg-16	–1.490	5.561×10^{-6}	0.13
Mg-Chi(Zn/BMP2)	–1.418	3.258×10^{-6}	0.08
Mg-Chi(Zn/BMP2)/HA	–1.408	2.582×10^{-6}	0.06

Figure 3b shows the electrochemical impedance spectra (EIS) of the control and modified magnesium alloys. Only one high frequency capacitive ring can be observed for Mg, Mg-OH, and Mg-16, respectively. For Mg-Chi(Zn/BMP2) and Mg-Chi(Zn/BMP2)/HA, both of high and low frequency

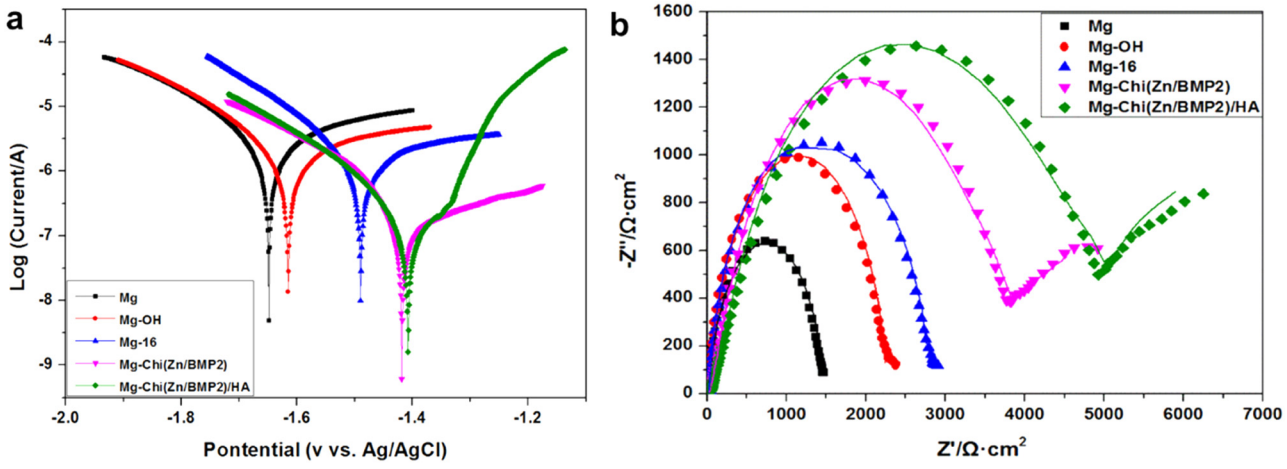

Figure 3: The electrochemical polarization curves and electrochemical impedance spectra (EIS) of the different samples.

capacitive rings existed on EIS spectra. As known, the high and low frequency rings correspond to the processes of charge transfer and mass transfer, respectively [37,38]. The radius of capacitive rings determined the corrosion resistance. The radius of high frequency ring was increased in sequence of Mg, Mg-OH, Mg-16 Mg-Chi(Zn/BMP2), and Mg-Chi(Zn/BMP2)/HA, indicating that the charge transfer became difficult and the corrosion resistance was gradually improved. For Mg-Chi(Zn/BMP2) and Mg-Chi(Zn/BMP2)/HA, the occurrence of low frequency rings indicated the mass transfer also slowed down. Therefore, it can be concluded that the corrosion resistance of magnesium alloy was gradually improved by the coating.

Figure 4 shows the curves of pH changes and Mg^{2+} release concentrations of the medium as a function of immersion time. As magnesium alloy was immersed into the SBF solution, lots of hydroxyl ions and magnesium ions were released due to the reaction of magnesium alloy with H_2O in aqueous solution, which resulted in the increase of pH values and Mg^{2+} concentrations. In 1 day, the pH values and Mg^{2+} concentrations of the medium for the control magnesium alloy increased rapidly and always presented the largest among all samples over 7 days, as shown in Figure 4, suggesting that the blank magnesium alloy was rapidly degraded in aqueous solution. For Mg-OH, although the degradation was hindered to some extent by the protective layers, the pH values and Mg^{2+} concentrations were still high on 7th day. In this case, the $Mg(OH)_2$ layer, formed by the alkali heat treatment, could inhibit the corrosion of the magnesium alloy. However, the existence of chloride ions in solutions would transfer $Mg(OH)_2$ into the more soluble $MgCl_2$. Upon losing the protective effect of the $Mg(OH)_2$ layer, the magnesium alloys would be further corroded, leading to high pH values and Mg^{2+} concentrations. For Mg-16, due to the covering effect of organic molecules, the transfer process of $Mg(OH)_2$ to $MgCl_2$ was slowed down to some extent. Thus, the overall pH and Mg^{2+} concentrations were decreased. After immobilizing Chi(Zn/BMP2) and Chi(Zn/BMP2)/HA on the surface, the pH values and Mg^{2+} concentrations were obviously decreased as compared to Mg, Mg-OH, and Mg-16, but gradually increased with the increasing immersion time, which can be attributed to the protective role of the chitosan membrane in the complex coating. It is worth noting that Mg^{2+} concentrations further decreased and merely reached 12.42 μg/mL after 7-days immersion for Mg-Chi(Zn/BMP2)/HA. This suggested that HA in the coating further slowed down the degradation rate of magnesium alloy.

3.4 Osteoblasts adhesion and growth behaviors

In order to investigate the adhesion and growth behaviors of osteoblasts on the surfaces of the control and modified magnesium alloys, the cells were stained with rhodamine and DAPI to obtain visible green cytoplasm and blue nucleus under a fluorescence microscope, respectively. Figure 5 illustrates the adhesion and spreading of osteoblasts for 1 and 3 days, respectively. Additionally, in order to evaluate the proliferation of osteoblast cells on different surfaces, the CCK-8 test was performed and the results are presented in Figure 6a. For the control Mg, severe corrosion and degradation of magnesium alloy took place in the culture medium, contributing to the

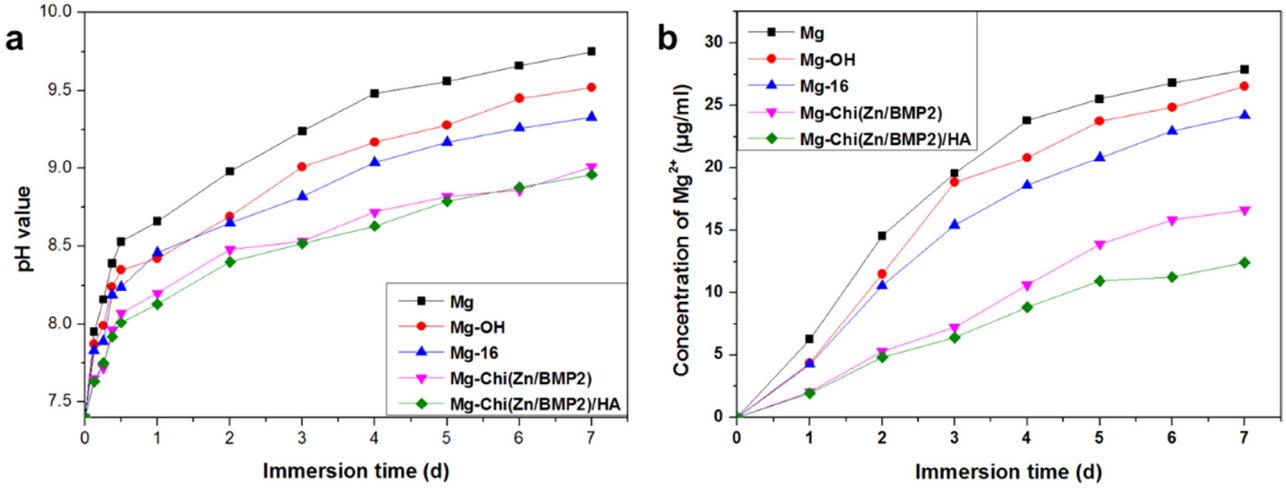

Figure 4: The degradable behaviors of the different samples characterized by pH changes and Mg^{2+} release concentrations of the medium.

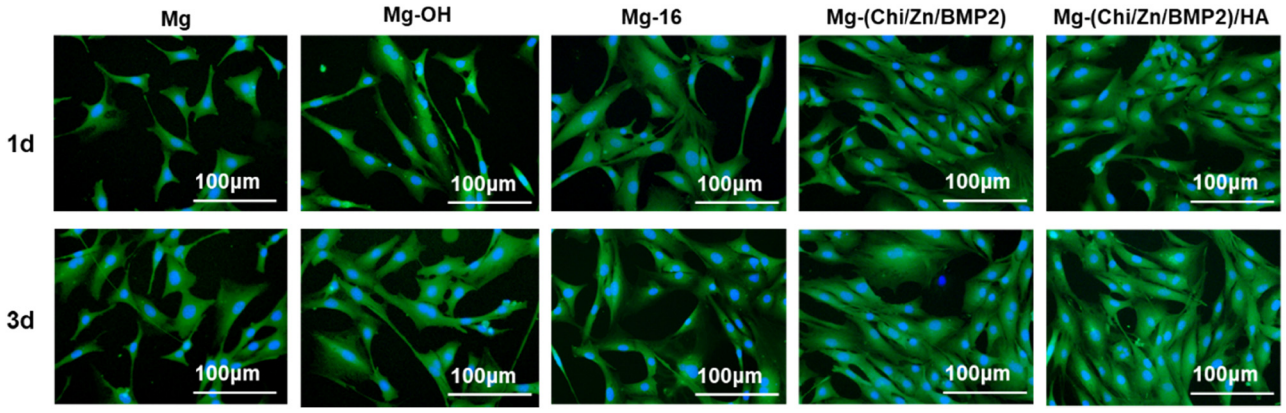

Figure 5: Fluorescence staining of osteoblasts on different surfaces after being cultured for 1 and 3 days, respectively (green: cytoplasm, blue: nucleus).

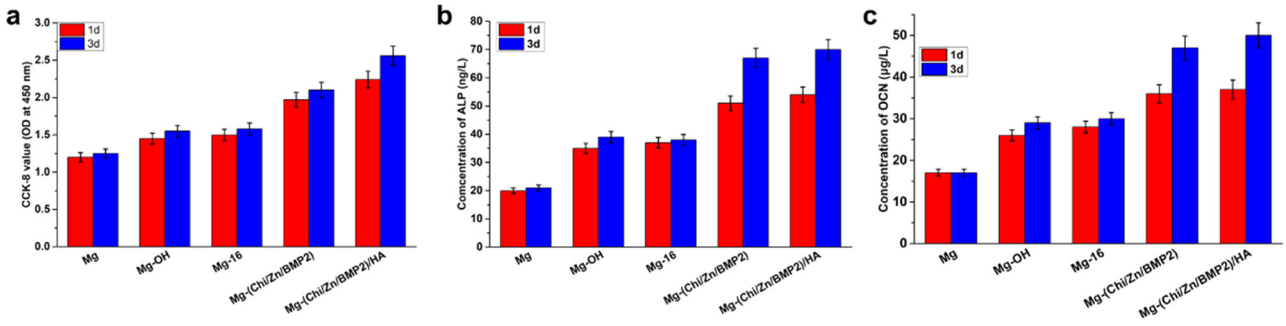

Figure 6: (a) Proliferation of osteoblast cells on different surfaces after 1 and 3 days evaluated by CCK-8 test. (b) and (c) show the ALP and OCN activities of osteoblast cells on different surfaces after culture 1 and 3 days, respectively. Data presented as mean ± SD (n = 3) and analyzed using one-way ANOVA.

appearance of bubbles and the increase of pH value (as shown in Figure 4). This was not beneficial to the adhesion, spreading, and proliferation of osteoblasts. Therefore, merely a bit of osteoblasts emerged on the samples both for 1- and 3-days culture. There was almost no visible difference between CCK-8 values. For Mg-OH, the alkali heat treatment induced the formation of $Mg(OH)_2$ layers and then enhanced the hydrophilicity and corrosion resistance of the surface to some degree. The cytocompatibility was improved by $Mg(OH)_2$ layers. But $Mg(OH)_2$ can be dissolved by Cl^- in the medium. Thus, it can be seen that the number of osteoblasts was slightly increased. The similar situation also appeared in the case of Mg-16. After self-assembly, the phosphating of the magnesium alloy from 16-phosphonyl-hexadecanoic acid suppressed the corrosion of Cl^-. Compared with Mg, the number of osteoblasts was increased on Mg-16 surface. The differences of CCK-8 values between 1 and 3 days slightly increased for Mg-OH and Mg-16. For Mg-Chi(Zn/BMP2) and Mg-Chi(Zn/BMP2)/HA, because of a good biological activity of the chitosan [29,30], a better osteogensis/osseointegration role of BMP2 [27], and improved corrosion resistance of the coating, the amount of osteoblasts was obviously increased. The osteoblast cells on the surfaces presented more spreading and increased binding sites. Besides, HA also possessed a good biocompatibility and promoted the growth of osteoblasts [31]. On the 3rd day, almost the whole surface was covered by the osteoblasts for Mg-Chi(Zn/BMP2)/HA, demonstrating that the cytocompatibility was further improved by the complex coating. The differences of CCK-8 values between 1 and 3 days can be evidently found, especially for Mg-(Chi/Zn/BMP2)/HA.

Figure 6b and c show the ALP (alkaline phosphatase) and OCN (osteocalcin) activities of osteoblast cells on different surfaces after 1 and 3 days, respectively. ALP and OCN are specific factors of osteoblast differentiation, marking the beginning of differentiation and maturation of osteoblasts, respectively. Therefore, the expression of ALP and OCN activities can be used as the criterion to

elevate the function of the coating on osteoblasts. For the control Mg, excessive corrosion and corrosion products on surfaces destroyed or even killed osteoblasts. Their ALP and OCN activities were lowest among all samples. Almost no significant difference can be found between 1 and 3 days. It can be said that the functional expression of osteoblast cells was seriously inhibited over time on the surface of Mg. After alkali heat treatment and self-assembly, the concentrations of ALP and OCN were slightly increased and only small differences can be found between 1 and 3 days. Compared with the control Mg, the ameliorative corrosion resistance of Mg-OH and Mg-16 facilitated osteoblast differentiation. However, owing to the lack of biological activity of Mg-OH and Mg-16, the complex containing BMP2 was immobilized onto magnesium alloy surfaces. BMP2 can stimulate DNA synthesis and cell replication, thereby promoting the directional differentiation of mesenchymal cells into osteoblasts. BMP2 is also the main factor that induces bone and cartilage formation in the body and is expressed in limb growth, endochondral ossification, early fracture, and cartilage repair. It plays an important role in the embryonic development and regeneration of bones [27]. In addition, zinc can stimulate bone formation and increase osteogenetic function in osteoblasts through exciting cell proliferation, ALP activity, collagen synthesis, and protein synthesis [39]. After the introduction of Chi(Zn/BMP2) and Chi(Zn/BMP2)/HA, the release of zinc ions and BMP2 remarkably elevated the early-stage and late osteogenic differentiation markers ALP and OCN, especially on the 3rd day. ALP reached 67 ng/L and 70 ng/L for Mg-Chi(Zn/BMP2) and Mg-Chi(Zn/BMP2)/HA, respectively. OCN were 47 μg/L and 52 μg/L for Mg-Chi(Zn/BMP2) and Mg-Chi(Zn/BMP2)/HA, respectively. It can be said that the complex coatings promoted the differentiation and functional expression of osteoblasts. HA (hydroxyapatite) is the main inorganic mineral component of human bones. Hydroxyl in HA can combine with water molecules, polysaccharide, protein, *etc*. in cells by hydrogen bonds, which is conducive to osteoblast adhesion [40]. In addition, the concave-convex structure of Mg-Chi(Zn/BMP2)HA coating gave osteoblasts more adhesion points [40]. HA can be dissolved to release Ca and P under the action of ALP, promoting the formation of new bone. In return, ALP activity was increased by HA, as shown in Figure 6b. It has been reported that HA can induce the formation of osteoblasts [40]. In summary, the Chi(Zn/BMP2)/HA coating was more beneficial for osteoblasts spreading and stimulating osteogenic differentiation.

3.5 Antibacterial activities

In order to investigate the antibacterial activities of the modified coatings, *Escherichia coli* (*E. coli*) was cultured on the surface of magnesium alloy before and after modification. The adhesion and proliferation of *E. coli* were also inspected. The results of typical SEM images and photographs of *E. coli* colonization are illustrated in Figure 7. Clearly, a large number of visible *E. coli* adhered to the surface of the control Mg and Mg-OH. It is suggested that Mg and Mg-OH as implant materials have great potential to be infected by bacteria. After 24 h of culture, the number of colonies in petri dish reached 3,648 and 3,997 for Mg and Mg-OH, respectively. Compared with the control

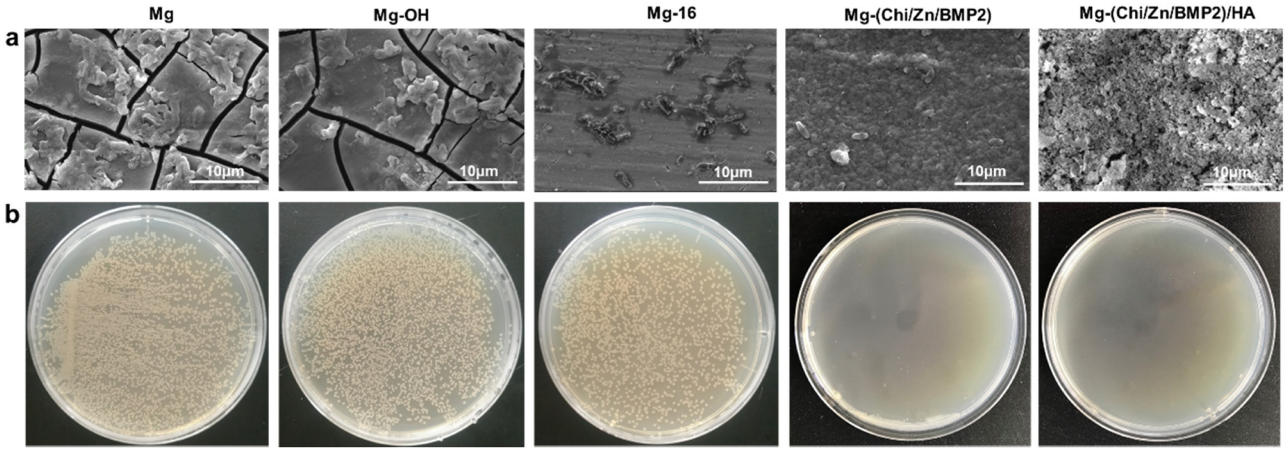

Figure 7: Typical SEM images (a) and photographs of colonization (b) by *E. coli* on different surfaces of magnesium alloy.

Mg, Mg-OH coating enhanced the corrosion resistance of magnesium alloy to a certain extent, but the number of colonies was more than that of Mg. This was most likely ascribed to the fast corrosion for Mg, which affected the survival environment of bacteria, and as a result, inhibited their growth [22]. Besides, the adhesion of *E. coli* was still severe for Mg-16. It is indicated that the improved corrosion resistance of Mg-OH and Mg-16 had limited effect on antibacterial properties. Similar results were also obtained in the previous report on antibacterial ability of coated and uncoated AZ31 alloy [22]. For Mg-Chi(Zn/BMP2) and Mg-Chi(Zn/BMP2)/HA, the amount of *E. coli* and its colonies was noticed to decrease significantly. As reported, the chitosan from the coatings can destroy the membrane structures of *E. coli* through interacting with proteins on the cell membrane [41]. The chitosan changed the permeability of membrane and caused cellular leakage [41]. Simultaneously, the released Zn^{2+} from the coatings had a significant effect in the active transport inhibition as well as in the amino acid metabolism and enzyme system disruption of *E. coli* [39]. Therefore, the synergistic antibacterial effect of chitosan and released Zn^{2+} led to the decreasing of bacterial adhesion and proliferation.

4 Conclusion

In order to solve the problems of too fast degradation rate, limited biocompatibility, and poor antibacterial effect of magnesium alloy, a multifunctional bioactive coating of Chi(Zn/BMP2)/HA was successfully constructed on surfaces. Compared with other samples, Mg-Chi(Zn/BMP2)/HA significantly enhanced the hydrophilicity and corrosion resistance. The Chi(Zn/BMP2)/HA coating also showed excellent biocompatibilities, which can not only significantly promote the osteoblast adhesion and proliferation, but also upregulate ALP and OCN expression of osteoblasts. Furthermore, due to the synergistic antibacterial effect of zinc ions and chitosan, Mg-Chi(Zn/BMP2)/HA had good antibacterial properties against *E. coli*. Therefore, the method in present study can be effectively used for the surface modification of magnesium alloys as orthopedic materials to simultaneously improve the corrosion resistance, biocompatibility, and antibacterial properties against *E. coli*. In future, implantation experiments with magnesium alloy coated with Chi(Zn/BMP2)/HA complex need to be performed to further verify the *in vivo* biocompatibility.

Funding information: The authors acknowledge the financial supports from the National Natural Science Foundation of China (31870952, 51701079), Natural Science Foundation of Jiangsu Province of China (BK20181480), Natural Science Foundation of Jiangsu Higher Education Institution of China (19KJB430013), the Innovation Project of Huai'an Municipal Science and Technology Bureau (HAB201844), and Postgraduate Science and Technology Innovation Training Project of HYIT (HGYK202107).

Author contributions: All authors have accepted responsibility for the entire content of this manuscript and approved its submission.

Conflict of interest: The authors state no conflict of interest.

References

[1] Wang JL, Xu JK, Hopkins C, Chow DHK, Qin K. Biodegradable magnesium-based implants in orthopedics – a general review and perspectives. Adv Sci. 2020;7(8):1902443.
[2] Zeng RC, Dietzel W, Witte F, Hort N, Blawert C. Progress and challenge for magnesium alloys as biomaterials. Adv Eng Mater. 2008;10(8):B3–14.
[3] Staigera MP, Pietaka AM, Huadmaia J, Dias G. Magnesium and its alloys as orthopedic biomaterials: A review. Biomaterials. 2006;27(9):1728–34.
[4] Nagels J, Stokdijk M, Rozing PM. Stress shielding and bone resorption in shoulder arthroplasty. J Shoulder Elb Surg. 2003;12(1):35–9.
[5] Lhotka C, Szekeres T, Steffan I, Zhuber K, Zweymuller K. Four-year study of cobalt and chromium blood levels in patients managed with two different metal-on-metal total hip replacements. J Orthop Res. 2003;21(2):189–95.
[6] Wu SL, Liu XM, Yeung KWK, Guo H, Li PH, Hu T, et al. Surface nano-architectures and their effects on the mechanical properties and corrosion behavior of Ti-based orthopedic implants. Surf Coat Tech. 2013;233(25):13–26.
[7] Zhou H, Liang B, Jiang HT, Deng ZL, Yu KX. Magnesium-based biomaterials as emerging agents for bone repair and regeneration: from mechanism to application. J Magnes Alloy. 2021;9(3):779–804.
[8] Nabiyouni M, Brückner T, Zhou H, Gbureck U, Bhaduri SB. Magnesium-based bioceramics in orthopedic applications. Acta Biomater. 2018;66(15):23–43.
[9] Zhao DW, Huang SB, Lu FQ, Wang BJ, Yang L, Qin L, et al. Vascularized bone grafting fixed by biodegradable magnesium screw for treating osteonecrosis of the femoral head. Biomaterials. 2016;81:84–92.
[10] Witte F, Kaese V, Haferkamp H, Switzer E, Meyer-Lindenberg A, Wirth CJ, et al. In vivo corrosion of four magnesium alloys and

the associated bone response. Biomaterials. 2005;26(17):3557–62.
[11] Tang HY, Wang F, Li D, Gu XN, Fan YB. Mechanical properties, degradation behaviors and biocompatibility of micro-alloyed Mg-Sr-RE alloys for stent applications. Mater Lett. 2020;264(1):127285.
[12] Wang J, Giridharan V, Shanov V, Xu ZG, Collins B, White L, et al. Flow-induced corrosion behavior of absorbable magnesium-based stents. Acta Biomater. 2014;10(12):5213–23.
[13] Witte F, Kaese V, Haferkamp H, Switzer E, Meyer-Lindenberg A, Wirth CJ, et al. In vivo corrosion of four magnesium alloys and the associated bone response. Biomaterials. 2005;26(17):3557–62.
[14] Noviana D, Paramitha D, Ulum MF, Hermawan H. The effect of hydrogen gas evolution of magnesium implant on the post-implantation mortality of rats. J Orthop Transl. 2016;5:9–15.
[15] Song GL. Control of biodegradation of biocompatable magnesium alloys. Corros Sci. 2007;49(4):1696–701.
[16] Wu GS, Ibrahim JM, Chu PK. Surface design of biodegradable magnesium alloys – a review. Surf Coat Tech. 2013;233(25):2–12.
[17] Gao F, Hu YD, Li GC, Liu S, Quan L, Yang ZM, et al. Layer-by-layer deposition of bioactive layers on magnesium alloy stent materials to improve corrosion resistance and biocompatibility. Bioact Mater. 2020;5(3):611–23.
[18] Gao JL, Su YC, Qin YX. Calcium phosphate coatings enhance biocompatibility and degradation resistance of magnesium alloy: Correlating in vitro and in vivo studies. Bioact Mater. 2021;6(5):1223–9.
[19] Wei X, Li ZC, Liu PD, Li SJ, Peng XB, Deng RP, et al. Improvement in corrosion resistance and biocompatibility of AZ31 magnesium alloy by NH^{2+} ions. J Alloy Compd. 2020;824(25):153832.
[20] Wu W, Sun X, Zhu CL, Zhang F, Zeng RC, Zou YH, et al. Biocorrosion resistance and biocompatibility of Mg–Al layered double hydroxide/poly-L-glutamic acid hybrid coating on magnesium alloy AZ31. Prog Org Coat. 2020;147:105746.
[21] Xue K, Liang LX, Cheng SC, Liu HP, Cui LY, Zeng RC, et al. Corrosion resistance, antibacterial activity and drug release of ciprofloxacin-loaded micro-arc oxidation/silane coating on magnesium alloy AZ31. Prog Org Coat. 2021;158:106357.
[22] Wang X, Yan HG, Hang RQ, Shi HX, Wang LF, Ma JC, et al. Enhanced anticorrosive and antibacterial performances of silver nanoparticles/polyethyleneimine/MAO composite coating on magnesium alloys. J Mater Res Tech. 2021;11:2354–64.
[23] Feng H, Wang G, Jin W, Zhang X, Huang Y, Gao A, et al. Systematic study of inherent antibacterial properties of magnesium-based biomaterials. ACS Appl Mater Interfaces. 2016;8(15):9662–73.
[24] Lin Z, Wu S, Liu X, Qian S, Chu PK, Zheng Y, et al. A surface-engineered multifunctional TiO_2 based nano-layer simultaneously elevates the corrosion resistance, osteoconductivity and antimicrobial property of a magnesium alloy. Acta Biomater. 2019;99:495–513.
[25] Brooks EK, Ahn R, Tobias ME, Hansen LA, Luke-Marshall NR, Wild L, et al. Magnesium alloy AZ91 exhibits antimicrobial properties in vitro but not in vivo. J Biomed Mater Res Part B. 2018;106B:221–7.
[26] Liang T, Zeng LL, Shi YZ, Pan HB, Chu PK, Yeung KWK, et al. In vitro and in vivo antibacterial performance of Zr & O PIII magnesium alloys with high concentration of oxygen vacancies. Bioact Mater. 2021;6(10):3049–61.
[27] Tao BL, Deng YM, Song LY, Ma WW, Qian Y, Lin CC, et al. BMP2-loaded titania nanotubes coating with pH-responsive multilayers for bacterial infections inhibition and osteogenic activity improvement. Colloid Surf B. 2019;177(1):242–52.
[28] Lin ZS, Sun XT, Yang HZ. The role of antibacterial metallic elements in simultaneously improving the corrosion resistance and antibacterial activity of magnesium alloys. Mater Des. 2021;198(15):109350.
[29] Seidi F, Yazdi MK, Jouyandeh M, Dominic M, Naeim H, Nezhad MN, et al. Chitosan-based blends for biomedical applications. Int J Biolo Macromol. 2021;183:1818–50.
[30] Zargar V, Asghari M, Dashti A. A review on chitin and chitosan polymers: structure, chemistry, solubility, derivatives, and applications. Chem Bio Eng Rev. 2015;2(3):204–26.
[31] Du MZ, Chen JD, Liu KH, Xing HR, Song C. Recent advances in biomedical engineering of nano-hydroxyapatite including dentistry, cancer treatment and bone repair. Compos Part B Eng. 2021;215:108790.
[32] Ho YH, Man K, Joshi SS, Pantawane MV, Wu TC, Yang Y, et al. In-vitro biomineralization and biocompatibility of friction stir additively manufactured AZ31B magnesium alloy-hydroxyapatite composites. Bioact Mater. 2020;5(4):891–901.
[33] Pan CJ, Hu YD, Hou Y, Liu T, Lin YB, Ye W, et al. Corrosion resistance and biocompatibility of magnesium alloy modified by alkali heating treatment followed by the immobilization of poly (ethylene glycol), fibronectin and heparin. Mater Sci Eng C. 2017;70:438–49.
[34] Hamil S, Baha M, Abdi A, Alili M, Bilican BK, Yilmaz BA, et al. Use of sea urchin spines with chitosan gel for biodegradable film production. Int J Biol Macromol. 2020;152:102–8.
[35] Gu XN, Zheng YF, Zhong SP, Xi TF, Wang JQ, Wang WH. Corrosion of, and cellular responses to Mg–Zn–Ca bulk metallic glasses. Biomaterials. 2010;31(6):1093–103.
[36] Zou YH, Wang J, Cui LY, Zeng RC, Wang QZ, Han QX, et al. Corrosion resistance and antibacterial activity of zinc-loaded montmorillonite coatings on biodegradable magnesium alloy AZ31. Acta Biomater. 2019;98:196–214.
[37] Zanotto F, Grassi V, Frignani A, Zucchi F. Protection of the AZ31 magnesium alloy with cerium modified silane coatings. Mater Chem Phys. 2011;129(1–2):1–8.
[38] Banerjee C, Woo RP, Grayson SM, Majumder A, Raman RKS. Influence of zeolite coating on the corrosion resistance of AZ91D magnesium alloy. Mater. 2014;7(8):6092–6104.
[39] Jin GD, Cao HL, Qiao YQ, Meng FH, Zhu HQ, Liu XY. Osteogenic activity and antibacterial effect of zinc ion implanted titanium. Colloid Surf B. 2014;117(1):158–65.
[40] Yang ZQ, Lei YK, Meng ZD. Therapeutic implication of nano-hydroxyapatite in orthopedics. Chin J Tissue Eng Res. 2012;16(51):9629–34.
[41] Kong M, Chen XG, Liu CS, Liu CG, Meng XH, Yu LJ. Antibacterial mechanism of chitosan microspheres in a solid dispersing system against E. coli. Colloid Surf B. 2008;65(2):197–202.